Mon. Not. R. Astron. Soc. **000**, 1–20 (2015) Printed 4 September 2015 (MN LATEX style file v2.2)

Luminosity and cooling of highly magnetised white dwarfs: Suppression of luminosity by strong magnetic fields

Mukul Bhattacharya[1,2⋆], Banibrata Mukhopadhyay[1]†, Subroto Mukerjee[1]‡
1. Department of Physics, Indian Institute of Science, Bangalore 560012, India
2. Department of Physics, University of Texas, Austin, TX 78712, USA

Accepted Received ; in original form

ABSTRACT

We investigate the luminosity and cooling of highly magnetised white dwarfs. We consider white dwarfs with electron-degenerate core and nondegenerate surface layers where cooling occurs by diffusion of photons. We find the temperature and density profiles in the surface layers or envelope of white dwarfs for radially constant and varying magnetic fields by solving the magnetostatic equilibrium and photon diffusion equations in a Newtonian framework. We also obtain the properties of white dwarfs at the core-envelope interface, when the core is assumed to be practically isothermal due to large thermal conductivity. With the increase in magnetic field, the interface temperature and density are found to be increasing. While the interface radius also increases with the increase in magnetic field when the field is hypothesised to be constant throughout the star, the interface radius decreases for varying fields. However, for white dwarfs having fixed interface radius or interface temperature, we find that the luminosity significantly decreases, falling in the range $\sim 10^{-6}-10^{-13}$ solar luminosity, with the increase in magnetic field strength at the interface and hence envelope, in the corresponding range $\sim 10^{9}-10^{11}$ G, in particular for the varying magnetic fields which are expected to be more realistic. This is remarkable as it argues for magnetised white dwarfs to be dimmer and be practically hidden in the H-R diagram. We also find the cooling rates corresponding to these luminosities. Interestingly, the decrease in temperature with time, for the fields under consideration, is not found to be appreciable — at most by a factor of two and that is also for the constant field cases.

Key words: stars: magnetic fields - white dwarfs - stars: luminosity function, mass function - MHD - stars: massive

1 INTRODUCTION

One of the most puzzling observations in high energy astrophysics in the last decade or so is that of the over-luminous type Ia supernova. More than a dozen such supernovae have been observed since 2006 (e.g. Howell et al. 2006; Scalzo et al. 2010), whose significantly high luminosities can only be justified by invoking very massive progenitors, of mass $M \geqslant 2M_{\odot}$ where $M_{\odot}$ is solar mass. However, the Chandrasekhar-limit prohibits the existence of such a massive progenitor white dwarf. Proposed models explaining these highly super-Chandrasekhar progenitors include rapidly (and differentially) rotating white dwarfs (Yoon & Langer 2004) and binary evolution of accreting differentially rotating white dwarfs (Hachisu 1986). Another set of proposals which has recently brought the issue of super-Chandrasekhar white dwarfs into the limelight relates to highly magnetised white dwarfs. In a series of papers, the main message of this work has been that the enormous power of a magnetic field — irrespective of its nature of origin: quantum (due to constant super-strong field: Kundu & Mukhopadhyay 2012; Das & Mukhopadhyay 2012, 2013; Das, Mukhopadhyay & Rao 2013), classical and/or general relativistic (due to a

⋆ mukulbhattacharya1993@gmail.com , mukul.b@utexas.edu
† bm@physics.iisc.ernet.in
‡ smukerjee@physics.iisc.ernet.in

varying strong field exerting magnetic pressure and tension: Das & Mukhopadhyay 2014a, 2015) — is capable of revealing significantly super-Chandrasekhar white dwarfs. Remarkably, unlike other proposals, this work also adequately predicts the required mass-range $2.1 - 2.8\ M_\odot$ of the progenitors in order to explain the set of over-luminous type Ia supernovae.

The impact of high magnetic fields not only lies in increasing the limiting mass of white dwarfs but it is also expected to change other properties including luminosity, temperature, cooling rate etc. Indeed, observations (Valyavin et al. 2014) argue for the suppression of cooling in white dwarfs due to strong magnetic fields. This is in particular due to suppression of convection over the entire surface of magnetised white dwarfs, which in turn hinders their cooling evolution. Therefore, highly magnetised white dwarfs may have lower surface temperature, and hence, luminosity. Nevertheless, poloidally dominated magnetised white dwarfs are shown to be smaller in size (Das & Mukhopadhyay 2015; Subramanian & Mukhopadhyay 2015), which can account for their lower luminosity.

Although magnetised white dwarfs were attempted to explore earlier (e.g. Ostriker & Hartwick 1968; Adam 1986), no author concentrated on the effects of magnetic fields on the internal properties of white dwarfs, e.g. thermal conduction, cooling rate etc. as well as luminosity, even though sometimes the chosen field was well above the critical field, $B_c = 4.414 \times 10^{13}$ G for Landau effects to arise (see, e.g., Adam 1986). The same is true for the exploration of magnetised white dwarfs by the Mukhopadhyay-group, mentioned above. Such an investigation has been more important for the magnetised white dwarfs proposed by the Mukhopadhyay group, because the underlying central fields could be stronger, sometimes $\gtrsim 5 \times 10^{15}$ G. Nevertheless, super-Chandrasekhar, magnetised white dwarfs were also explored with relatively weaker central fields, e.g. $\sim 5 \times 10^{14}$ G, which do not reveal any quantum mechanical effects, but the underlying magnetic pressure gradient, determined by the field geometries and profiles, is responsible for making the mass super-Chandrasekhar (Das & Mukhopadhyay 2014a, 2015; Subramanian & Mukhopadhyay 2015).

In the present paper, we study the cooling of magnetised white dwarfs and calculate the corresponding luminosities. While the cooling of white dwarfs is not a completely resolved issue, it has been investigated since 1950s, e.g., when Mestel (1952) attempted to understand the source of energy of white dwarfs and to estimate the ages of observed white dwarfs. Subsequently, Mestel & Ruderman (1967) also explored the cooling of white dwarfs and found them to be radiating at the expense of their thermal energy. They also showed, by including the Coulomb contribution to the thermal energy, that the lifetimes of white dwarfs are twice as large as estimated earlier. The evolution and cooling of low mass white dwarfs, beginning as a bright central star to the stage of crystallization after about 10 billion years, were also addressed by Tutukov & Yungelson (1996) who argued that the similarity of a modern cooling curve then to the one predicted by Mestel (1952) is the consequence of a series of accidents. Furthermore, Hansen (1999) reviewed the physics of cool white dwarfs, in particular their impact in order to extract valuable information about the early history of our galaxy.

The above works either did not consider the effects of magnetic field or the fields embedding the star were assumed to be too weak to have any practical effects. On the other hand, the field of magnetised white dwarfs considered by our group (and some others), as mentioned above, is high enough compared to that of all previous works which addressed the cooling of white dwarfs. Hence, here we plan to explore the cooling and luminosity of magnetised white dwarfs proposed by us earlier.

This paper is organized as follows. In §2, we recapitulate how the density and temperature profiles at the interface can be obtained for non-magnetised white dwarfs, in addition to computing their cooling timescales. In §3, we include the contribution of the magnetic field to the pressure and density of white dwarfs and compute the resultant density and temperature profiles for different luminosities and magnetic field strengths. Subsequently, in §4, we consider white dwarfs having either fixed interface radius or fixed interface temperature and evaluate their luminosities for increasing field strength. In §5, we compute the cooling rates of magnetised white dwarfs for the cases discussed in §4. Next, we discuss the implications of our results for non-magnetised and magnetised white dwarfs in §6. Finally, we conclude with a summary in §7.

2 TEMPERATURE PROFILE AND COOLING FOR A NON-MAGNETISED WHITE DWARF

In this section, we recapitulate how the luminosity-temperature relation and the temperature profile can be obtained using the equations of hydrostatic equilibrium and photon diffusion for a non-magnetised non-relativistic white dwarf having a nondegenerate ideal gas envelope. Once we know the luminosity and the specific heat in terms of temperature, we can find the cooling rate of the white dwarf. We use the same notation as used by Shapiro & Teukolsky (1983).

2.1 Density and temperature profiles in the surface layers

The electrons in the interior of a white dwarf are completely degenerate and have a large mean free path. This results in a high thermal conductivity and a uniform temperature in the inner regions (core) of the white dwarf. Nondegenerate surface layers, which form the envelope and are in "radiative equilibrium" with each other and cover the isothermal interior of the white dwarf. By radiative equilibrium, we mean that the matter is in thermodynamic equilibrium locally and energy flux is carried outward by photon diffusion.

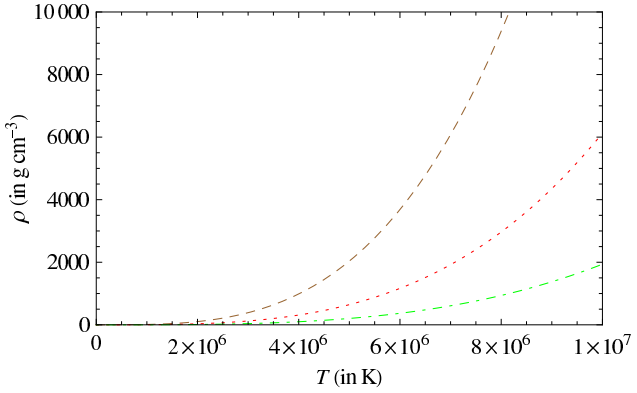

Figure 1. Variation of density with temperature for different luminosities: $10^{-5}L_\odot$ (dashed line), $10^{-4}L_\odot$ (dotted line) and $10^{-3}L_\odot$ (dot-dashed line), when $R = 5000$ km and $T_s = 5000$ K.

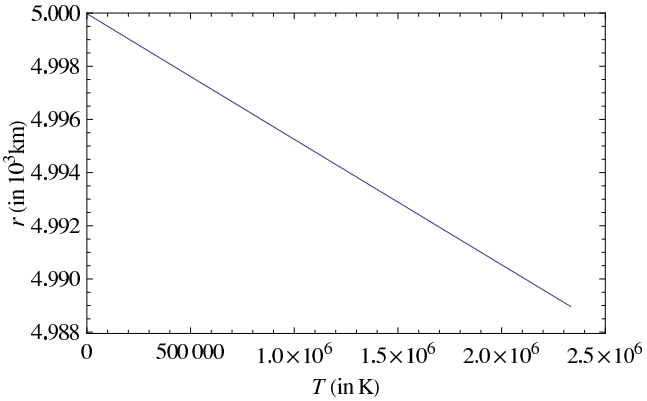

Figure 2. Variation of radius with temperature for luminosity $L = 10^{-5}L_\odot$, when $R = 5000$ km and $T_s = 5000$ K.

Using the equations for photon diffusion and hydrostatic equilibrium, we obtain,

$$\frac{dP}{dT} = \frac{4ac}{3}\frac{4\pi G m(r)}{\kappa L}T^3. \tag{1}$$

In the above equation, P is the pressure, T is the temperature, a is the radiation constant, c is the speed of light in vacuum, G is Newton's gravitational constant, $m(r)$ is the mass enclosed within radius r, κ is the opacity of the stellar material and L is the luminosity. The opacity can be approximated by Kramer's formula

$$\kappa = \kappa_0 \rho T^{-3.5}, \tag{2}$$

where $\kappa_0 = 4.34 \times 10^{24} Z(1+X)$ cm^{2}g^{-1} and ρ, X and Z are the density of the stellar material, mass fractions of hydrogen and heavy elements (elements other than hydrogen and helium) in the stellar interior, respectively (Schwarzschild 1958). The opacity is due to the bound-free and free-free transitions of electrons (Shapiro & Teukolsky 1983).

Surface layers are expected to be much thinner as compared to the radius of the white dwarf and therefore, $m(r) \approx M$ where, M is the mass of the white dwarf. Henceforth, the solar luminosity will be denoted as $L_\odot$ and the terms "surface layers" and "envelope" will be used interchangeably. In Eqn. (1), we substitute ρ using the equation of state (EoS) of nondegenerate matter (ideal gas) and integrate with the boundary condition $P = 0$ at $T = 0$ to obtain

$$\rho = \left(\frac{2}{8.5}\frac{4ac}{3}\frac{4\pi GM}{\kappa_0 L}\frac{\mu m_\mu}{k_B}\right)^{1/2} T^{3.25}, \tag{3}$$

where m_μ is the atomic mass unit, μ is the average mass of particles in units of m_μ and k_B is the Boltzmann constant. The above relation between ρ and T is valid only in the surface layers and breaks down for the degenerate core of the white dwarf. At the interface between the degenerate core and the nondegenerate envelope, the variation of density with temperature can be obtained, by equating the electron pressure on both sides, as

$$\rho_* \approx (2.4 \times 10^{-8}\ \mathrm{g\ cm^{-3}})\ \mu_e T_*^{3/2}. \tag{4}$$

where μ_e is the mean molecular weight per electron in units of m_μ. For a typical white dwarf, $X = 0$, the mass fraction of helium $Y = 0.9$, $Z = 0.1$ and $M \approx M_\odot$. Using $\mu_e \approx 2$, $\mu \approx 1.4$ and combining Eqns. (3) and (4), the luminosity at the interface can be written in terms of temperature as

$$L \approx (2 \times 10^6\ \mathrm{erg\ s^{-1}})\frac{M}{M_\odot}T_*^{3.5}. \tag{5}$$

Hence, the interface temperature of a white dwarf can be determined if L, M and the composition are known. For observed white dwarfs, $L \approx 10^{-5} - 10^{-2}L_\odot$ which corresponds to $T_* \approx 10^6 - 10^7$ K and $\rho_* \approx 10^2 - 10^3$ g cm^{-3}. Substituting the expression for ρ in the photon diffusion equation and integrating across the envelope, we obtain

$$T_* - T_s = \frac{1}{4.25}\frac{\mu m_\mu}{k_B}\frac{GM}{R}\left(\frac{R}{r_*} - 1\right), \tag{6}$$

where T_s is the temperature at the surface, with r_* and R being the radii of the interface and the surface, respectively.

We consider white dwarfs with $M = M_\odot$. Using the Chandrasekhar's relation for white dwarfs, this corresponds to radius, $R = 5000$ km (Chandrasekhar 1931a,b). We will consider this set of mass and radius throughout the paper. However, the results presented here practically do not change for other values of R (e.g., in the range $500 - 5000$ km) and M, unless T_s is as high as 10^5 K which we do not observe. Figures 1 and 2 show the variations of density and radius, respectively, with

temperature in the non-degenerate envelope. Figure 1 shows that the density at a given temperature, and hence radius, is suppressed with increasing luminosity. From Eqn. (6), it can be seen that the $T - r$ relation is independent of luminosity.

Hence, we obtain the relation to be of straight lines with the same slope for different values of luminosity, as shown in Fig. 2 for $L = 10^{-5} L_{\odot}$. As T_* is different for different luminosities, the corresponding $T - r$ lines originate from different temperatures at the interface.

With the increase of L, T_* increases whereas r_* decreases. For $T_* \approx 10^6 - 10^7$ K and $T_s \approx 10^3 - 10^4$ K,

$$\frac{r_*}{R} \geqslant 0.99. \tag{7}$$

Corresponding to $10^6 \leqslant T_* \leqslant 10^7$ K, we have $\rho_* \leqslant 1500\,\mathrm{g\,cm^{-3}} \ll \rho_c$, where ρ_c is the central density of the white dwarf. Table 1 shows the variations of T_*, ρ_* and r_* as L changes for a given value of T_s and R. We see that as L increases, T_* increases whereas r_* decreases.

Table 1: T_*, ρ_* and r_* for different L, when $T_s = 5000$ K and $R = 5000$ km

L (in $L_{\odot}$)	T_* (in K)	ρ_* (in g cm^{-3})	r_* (in R)	$\left\lvert\frac{\Delta T}{\Delta r}\right\rvert = \left\lvert\frac{T_* - T_s}{r_* - R}\right\rvert$ (in K cm^{-1})
10^{-5}	2.332×10^6	170.722	0.9978	2.1097
5×10^{-5}	3.69346×10^6	340.289	0.9965	2.11616
10^{-4}	4.50238×10^6	457.995	0.9958	2.11841
5×10^{-4}	7.13096×10^6	912.892	0.9933	2.12588
10^{-3}	8.69273×10^6	1228.66	0.9918	2.12935
5×10^{-3}	1.37677×10^7	2449.01	0.9871	2.14039
10^{-2}	1.6783×10^7	3296.13	0.9844	2.14662

Hence, as the luminosity of a non-magnetised white dwarf increases, the interface shifts inwards and the degenerate region shrinks in volume. However, for the observed range of luminosities, the decrease in volume of the degenerate region is quite small. Also $|\Delta T/\Delta r|$ increases with luminosity but does not vary appreciably with luminosity and is almost constant.

2.2 White dwarf cooling rate

Now, we recapitulate the discussion of white dwarf cooling as outlined by Mestel (1952) and Schwarzschild (1958). The thermal energy of the ions is the only significant source of energy that can be radiated when a star enters the white dwarf stage. As most of the electrons occupy the lower energy states in a degenerate gas, the thermal energy of the electron gas cannot be readily released. Also, the energy release from neutrino emission is considerable only in the very early phase when the temperature is high. The thermal energy of the ions and the rate at which it is transported to the surface and to be radiated are dependent on the specific heat, which in turn depends significantly on the physical state of the ions in the core as discussed below.

2.2.1 Crystallization and melting temperature

The discussion here is applicable to stars with ionic densities less than $10^6\,\mathrm{g\,cm^{-3}}$ as is the case for the white dwarfs we study. At very high temperatures, $T \gg 10^7$ K, and the ions are in a gaseous state with the kinetic energy of thermal motion large compared to the Coulomb energy. The specific heat per ion c_v is thus that of an ideal gas with $c_v = 3k_B/2$. As the ionic core cools, the gas starts deviating from its ideal behavior and the Coulomb energy can no longer be neglected. In the absence of any thermal motion, the configuration of the ions that minimizes the Coulomb energy is a lattice (with a BCC structure).

The ions here are no longer free like in an ideal gas and their kinetic energy corresponds to vibrations about the equilibrium positions of the lattice. An estimate of the temperature T_g below which the ions can no longer be thought of as being in a gaseous state is obtained by equating the kinetic energy with the vibrational energy yielding

$$T_g \approx 3 \times 10^4 \rho^{1/3} \tilde{Z}^{5/3} \text{ K}, \tag{8}$$

where $\tilde{Z}$ is the atomic number. Below T_g, the ionic system can be thought of as being in a liquid state. As the core cools further, the liquid crystallizes releasing its latent heat of melting which temporarily arrests further cooling. However, once this energy has been radiated, the cooling starts again and the ions eventually crystallize at a temperature T_m, which is the melting temperature of the Coulomb lattice. An estimate of T_m can be obtained from the Lindemann criterion (Lindemann 1910), which states that melting occurs when the root mean square displacement of the ions about their equilibrium positions due to thermal vibrations is about a quarter of the inter-ionic spacing. This gives

$$T_m \approx 2 \times 10^3 \rho^{1/3} \tilde{Z}^{5/3} \text{ K}. \tag{9}$$

Thermal vibrations of the ions correspond to excitations of the normal (phonon) modes of the ionic crystal. Below T_m, the distribution of energy in these modes can initially be thought of as being consistent with classical equipartition yielding $c_v = 3k_B$, which is the Dulong-Petit law. Upon further cooling, the quantization of the energy in each mode needs to be considered, and the specific heat is that of a quantum crystal. The temperature below which this happens is the Debye temperature θ_D of the lattice and is related to the the plasma frequency Ω_p of the ions as

$$\theta_D = \frac{\hbar}{k_B} \Omega_p \, , \tag{10}$$

where

$$\Omega_p = \left(\frac{4\pi n_i Z^2 e^2}{m_i} \right)^{1/2}. \tag{11}$$

Here n_i is the number density of the ions, m_i is the mass of a single ion, e is the charge of an electron and $\hbar$ is Planck's constant. For $T \ll \theta_D$,

$$c_v \approx \frac{16\pi^4}{5} \left(\frac{T}{\theta_D} \right)^3 k_B. \tag{12}$$

2.2.2 Time dependence of temperature

The cooling rate of a white dwarf is given by $-dU/dt$, which can be equated to the expression for L to give (Shapiro & Teukolsky 1983)

$$-\frac{d}{dt} \int c_v dT = C A m_\mu T^{7/2}, \tag{13}$$

where $CM_\odot \approx 2 \times 10^6 \text{ erg s}^{-1}$ and A is the atomic mass. For $T \gg T_g$, $c_v \sim 3k_B/2$, which gives

$$-\frac{d}{dt} \left(\frac{3k_B T/2}{A m_\mu} \right) = C T^{7/2}. \tag{14}$$

Integrating, we obtain

$$\frac{3}{5} \frac{k_B}{A m_\mu} \left(T^{-5/2} - {T_0}^{-5/2} \right) = C(t - t_0) = C\tau, \tag{15}$$

where T_0 is the initial temperature (before cooling starts), T is the present temperature at time t and $\tau = t - t_0$ is the age of the white dwarf. Using Eqn. (5) we rewrite Eqn. (15) as

$$\tau = \frac{3}{5} \frac{k_B M}{A m_\mu} \left(\frac{T}{L} - \frac{T_0}{L_0} \right) = \frac{3}{5} \frac{k_B M}{A m_\mu} \frac{T}{L} \left(1 - \left(\frac{T}{T_0} \right)^{5/2} \right), \tag{16}$$

where, L_0 and L are the initial and present luminosities of the white dwarf, respectively. Putting in the values of the constants in Eqn. (15), we have

$$T^{-5/2} - T_0^{-5/2} = 2.4058 \times 10^{-34} \tau. \tag{17}$$

Using Eqn. (17), we find the present temperature, T, and luminosity, L, at the interface for different values of τ which correspond to the present age of the white dwarf. We calculate T for T_* given in Table 1 and $\tau = 10$ billion years, i.e., 3.1536×10^{17} s. It is important to note that τ cannot exceed 13.8 billion years, which is the present age of the universe.

From Fig. 3, it can be seen that cooling at the interface is considerable only for higher values of luminosities ($L \geqslant 10^{-3} L_\odot$). The value of T_* remains almost constant for $L = 10^{-5} L_\odot$. Using Eqn. (5) in Eqn. (16), we obtain

$$\tau \propto \left(\frac{L^{-5/7} - {L_0}^{-5/7}}{M^{-5/7}} \right). \tag{18}$$

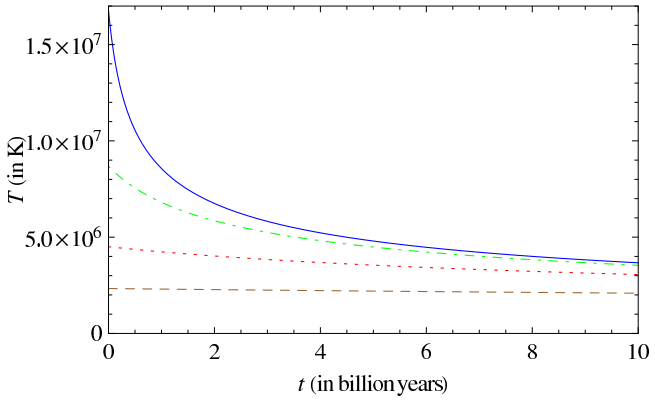

Figure 3. Variation of temperature with time for different initial luminosities: $10^{-5}L_\odot$ (dashed line), $10^{-4}L_\odot$ (dotted line), $10^{-3}L_\odot$ (dot-dashed line) and $10^{-2}L_\odot$ (solid line).

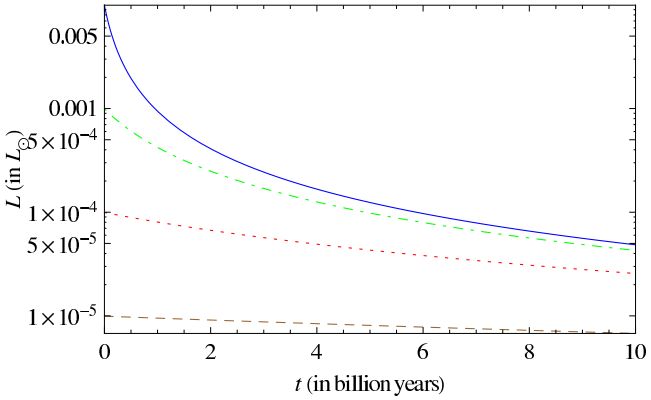

Figure 4. Variation of luminosity with time for different initial luminosities: $10^{-5}L_\odot$ (dashed line), $10^{-4}L_\odot$ (dotted line), $10^{-3}L_\odot$ (dot-dashed line) and $10^{-2}L_\odot$ (solid line).

Therefore, the luminosity and interface temperature both reduce with time, for a given initial luminosity of the white dwarf. From Fig. 4, it can be seen that even after 10 billion years, L decreases only by one order of magnitude. This explains why many white dwarfs have yet not faded from view, although their initial luminosities may have been quite low. Figure 3 shows that white dwarfs spend most of the time near their present temperature.

For $\theta_D \ll T \ll T_g$, $c_v \approx 3k_B$, which gives,

$$\tau = \frac{6}{5}\frac{k_B M}{A m_\mu}\left(\frac{T}{L} - \frac{T_0}{L_0}\right) = \frac{6}{5}\frac{k_B M}{A m_\mu}\frac{T}{L}\left(1 - \left(\frac{T}{T_0}\right)^{5/2}\right). \tag{19}$$

This τ is bigger than that in Eqn. (16) by a factor of 2, because of the inclusion of the lattice potential energy.

For $T \ll \theta_D$, using Eqn. (12), we obtain

$$\tau = \frac{128\pi^4}{5}\left(\frac{T}{\theta_D}\right)^3\left[\left(\frac{T_0}{T}\right)^{1/2} - 1\right]\frac{M k_B T}{A m_\mu L} = \frac{128\pi^4}{5}\frac{k_B M}{A m_\mu {\theta_D}^3}\left(\frac{T_0^4}{L_0} - \frac{T^4}{L}\right). \tag{20}$$

This is shorter than the classical result whenever $T \leqslant 0.1\theta_D$ (Mestel & Ruderman 1967). In this case, c_v falls off rapidly below θ_D, which leads to faster cooling and better agreement with observations.

We have neglected neutrino emission from the right-hand side of Eqn. (13). Thermal neutrino emission dominates over photon emission if $L \geqslant 10^{-0.5}L_\odot$ and $T \geqslant 10^{7.8}$ K (Shapiro & Teukolsky 1983). However, the luminosities that we consider here satisfy $L \leqslant 10^{-2}L_\odot$ and hence, photon emission dominates over thermal neutrino emission.

Moreover, convection might also result in shorter cooling timescales due to more efficient energy transfer. But Lamb & Van Horn (1975) and Fontaine & Van Horn (1976) showed that convection is not significant to a first approximation.

3 TEMPERATURE PROFILE IN THE PRESENCE OF A MAGNETIC FIELD

Here we solve the magnetostatic equilibrium and photon diffusion equations in the presence of a magnetic field (B) and investigate the change in the temperature profile inside a white dwarf. We perform our calculations for both radially constant and radially variable magnetic fields. Entire calculation is being performed in the same spirit as done for non-magnetised white dwarfs (e.g. Shapiro & Teukolsky 1983) above, except with the inclusion of magnetic fields. Hence, the hydrostatic equilibrium is replaced by the magnetostatic equilibrium.

The presence of B inside a white dwarf gives rise to an additional magnetic pressure, $P_B = \frac{B^2}{8\pi}$, which adds up with the electron degeneracy pressure to give rise to the total pressure. Furthermore, the density also has a contribution from the magnetic field which is given by, $\rho_B = \frac{B^2}{8\pi c^2}$. Such a situation can be tackled more ingeniously in the general relativistic framework rather than Newtonian framework. Nevertheless, here as a first approximation, we construct the magnetostatic equilibrium and photon diffusion equations in a Newtonian framework approximately as

$$\frac{d}{dr}(P + P_B) = -\frac{GM}{r^2}(\rho + \rho_B), \tag{21}$$

and

$$\frac{dT}{dr} = -\frac{3}{4ac}\frac{\kappa_0(\rho + \rho_B)^2}{T^{6.5}}\frac{L}{4\pi r^2}, \tag{22}$$

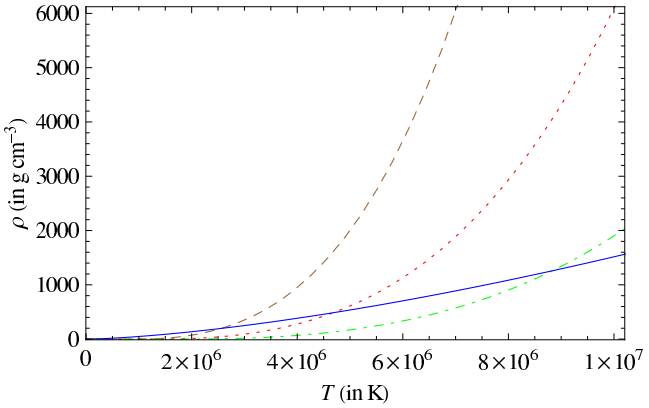

Figure 5. Variation of density with temperature for $B = 10^{12}$ G and different luminosities: $10^{-5}\,L_\odot$ (dashed line), $10^{-4}\,L_\odot$ (dotted line) and $10^{-3}\,L_\odot$ (dot-dashed line). ρ_* and T_* are obtained from the intersection of $\rho - T$ profiles with Eqn. (4) (solid line).

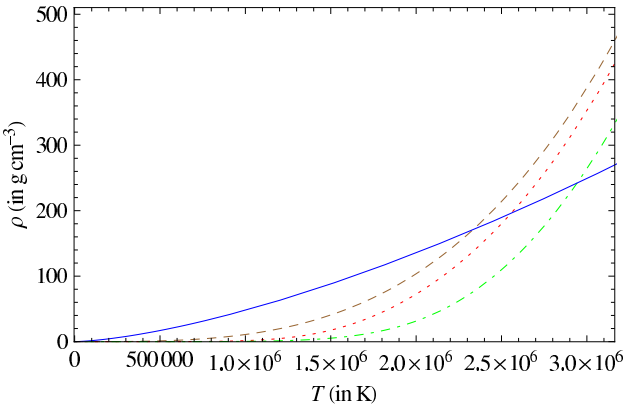

Figure 6. Variation of density with temperature for $L = 10^{-5}\,L_\odot$ and different magnetic fields: 10^{10} G (dashed line), 10^{12} G (dotted line) and 2×10^{12} G (dot-dashed line). ρ_* and T_* are obtained from the intersection of $\rho - T$ profiles with Eqn. (4) (solid line).

respectively, neglecting magnetic torsion terms. Using Eqns. (21) and (22), we can write

$$\frac{d}{dT}\left(P + \frac{B^2}{8\pi}\right) = \frac{4ac}{3}\frac{4\pi GM}{\kappa_0 L}\frac{T^{6.5}}{\left(\rho + \frac{B^2}{8\pi c^2}\right)}. \tag{23}$$

It has already been shown that including the effects of a magnetic pressure gradient and magnetic density gives rise to stable highly super-Chandrasekhar white dwarfs (Das & Mukhopadhyay 2014a,b, 2015). Note that a large number of magnetised white dwarfs with surface fields as high as 10^9 G have been discovered by the Sloan Digital Sky Survey (SDSS) (Schmidt et al. 2003). It is possible that their central field is several orders of magnitude larger than the surface field. To capture the variation of B, we use a profile proposed by Bandyopadhyay et al. (1997), modeling B as a function of ρ, given by

$$B\left(\frac{\rho}{\rho_0}\right) = B_s + B_0\left[1 - \exp\left(-\eta\left(\frac{\rho}{\rho_0}\right)^\gamma\right)\right], \tag{24}$$

where B_s is the surface magnetic field, B_0 is a parameter having dimension of B, η and γ are parameters determining how the magnetic field decays from the core to the surface. The value of ρ_0 is chosen to be ten percent of ρ_c. We set, $\eta = 0.8$, $\gamma = 0.9$ and $\rho_0 = 10^9$ g cm^{-3} for all our calculations. Close to the surface, we have $\rho \to 0$ and therefore $B \to B_s$.

In §3.1, we first find the temperature profile in the presence of a constant radial magnetic field by setting $B_0 = 0$ and choosing various values of B_s, so that the magnetic field is independent of ρ. Then in §3.2, we vary both B_0 and B_s to find the temperature profile for a radially varying field.

3.1 Constant magnetic field

By constant magnetic field, we mean a magnetic field independent of ρ and having the same magnitude throughout the white dwarf. This is somewhat of an ideal case, but is a good choice to start the investigation. For this, we set $B_0 = 0$ which gives $B = B_s =$ constant and choose L such that $10^{-5}L_\odot \leqslant L \leqslant 10^{-2}L_\odot$ is satisfied. We consider a white dwarf with mass $M = M_\odot$ and vary the magnitudes of B_s and L to check how T_*, r_* and the temperature profile in the envelope change.

As we are interested in the surface layers which are nondegenerate, we can substitute for P in terms of ρ in Eqn. (23) by using the ideal gas equation of state to obtain

$$\frac{d}{dT}\left(\frac{\rho k_B T}{\mu m_\mu}\right) = \frac{4ac}{3}\frac{4\pi GM}{\kappa_0 L}\frac{T^{6.5}}{\left(\rho + \frac{B^2}{8\pi c^2}\right)}. \tag{25}$$

Putting in the values of the constants and using $Z = 0.1$ and $X = 0$, we have

$$5.938 \times 10^7\rho + 5.938 \times 10^7 T\frac{d\rho}{dT} = \frac{1.168}{L}\frac{T^{6.5}}{\left(\rho + \frac{B^2}{2.261\times10^{22}}\right)}. \tag{26}$$

From Eqn. (22), we have

$$\frac{dr}{dT} = -8.758 \times 10^{-27}\frac{T^{6.5}}{\left(\rho + \frac{B^2}{8\pi c^2}\right)^2}\frac{r^2}{L}. \tag{27}$$

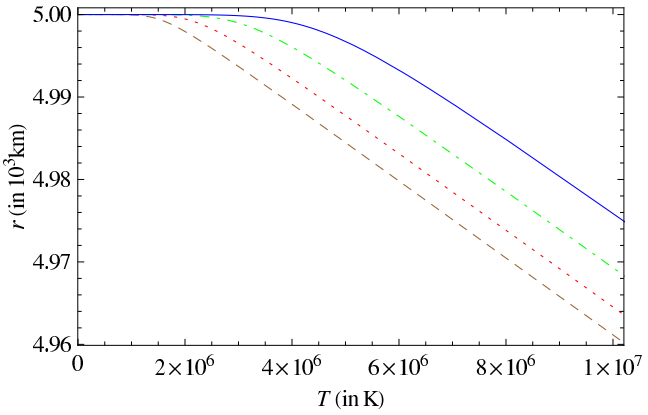

Figure 7. Variation of radius with temperature for $B = 10^{12}$ G and different luminosities: $10^{-5}\,L_\odot$ (dashed line), $10^{-4}\,L_\odot$ (dotted line), $10^{-3}\,L_\odot$ (dot-dashed line) and $10^{-2}\,L_\odot$ (solid line).

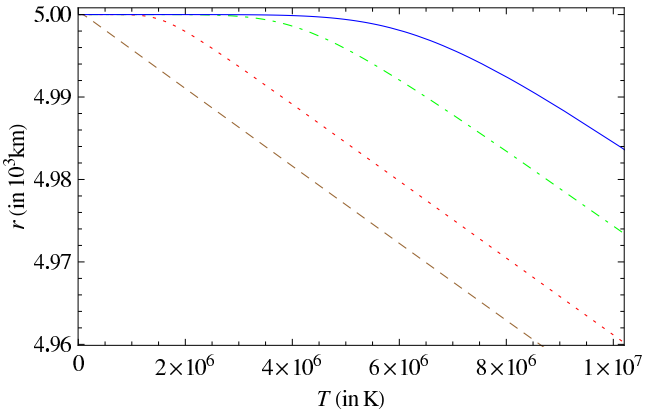

Figure 8. Variation of radius with temperature for $L = 10^{-5}\,L_\odot$ and different magnetic fields: 10^{10} G (dashed line), 10^{12} G (dotted line), 5×10^{12} G (dot-dashed line) and 10^{13} G (solid line).

Table 2: Interface temperature (in K) for different luminosities and magnetic fields

L	$10^{-5}\,L_\odot$	$10^{-4}\,L_\odot$	$10^{-3}\,L_\odot$	$10^{-2}\,L_\odot$
$B = 0$	2.332×10^6	4.50238×10^6	8.69273×10^6	1.6783×10^7
$B = 10^{10}$ G	2.33202×10^6	4.5024×10^6	8.69275×10^6	1.6783×10^7
$B = 10^{11}$ G	2.33478×10^6	4.50439×10^6	8.69418×10^6	1.67841×10^7
$B = 10^{12}$ G	2.5559×10^6	4.68586×10^6	8.83246×10^6	1.68858×10^7
$B = 5 \times 10^{12}$ G	3.92503×10^6	6.41893×10^6	1.07706×10^7	1.8764×10^7
$B = 10^{13}$ G	5.07388×10^6	8.14314×10^6	1.32226×10^7	2.19241×10^7
$B = 5 \times 10^{13}$ G	9.54829×10^6	1.51536×10^7	2.40817×10^7	3.83716×10^7
$B = 10^{14}$ G	1.25884×10^7	1.99615×10^7	3.16693×10^7	5.02952×10^7
$B = 5 \times 10^{14}$ G	2.39528×10^7	3.79647×10^7	6.01765×10^7	9.53938×10^7

We solve Eqns. (26) and (27) simultaneously by specifying boundary conditions at the surface as

$$\rho(T_s) = \rho_s = 10^{-10}\ \mathrm{g\,cm^{-3}},\ \ r(T_s) = R = 5000\ \mathrm{km},\ T_s = 5000\ \mathrm{K}. \tag{28}$$

Once we obtain $\rho - T$ and $r - T$ profiles for the given boundary conditions, we can find T_* and ρ_* by solving $\rho - T$ profile along with Eqn. (4), as shown in Figs. 5 and 6. This works because the $\rho - T$ profile is valid in the whole envelope whereas Eqn. (4) is valid only at the interface. Once we know T_*, we can also find r_* from the $r - T$ profile, as shown in Figs. 7 and 8.

In Tables 2, 3 and 4, we present the values of T_*, ρ_* and r_* respectively for different values of B and L. The values of T_*, ρ_* and r_* have been specified to high precision (up to higher decimal places), as the temperature after cooling is quite sensitive to the initial conditions. We see that T_* and ρ_* increase with both B and L. For a given B, T_* becomes almost twice in magnitude as L increases by one order of magnitude. Also, r_* decreases with an increase in L for a given B. Therefore, the interface moves inwards with increase in L for a given B.

Table 3: Interface density (in $\mathrm{g\,cm^{-3}}$) for different luminosities and magnetic fields

L	$10^{-5}\,L_\odot$	$10^{-4}\,L_\odot$	$10^{-3}\,L_\odot$	$10^{-2}\,L_\odot$
$B = 0$	170.722	457.995	1228.66	3296.13
$B = 10^{10}$ G	170.725	457.998	1228.67	3296.13
$B = 10^{11}$ G	171.028	458.302	1228.97	3296.43
$B = 10^{12}$ G	195.891	486.275	1258.41	3326.46
$B = 5 \times 10^{12}$ G	372.789	779.635	1694.55	3896.59
$B = 10^{13}$ G	547.908	1114	2305.01	4921.32
$B = 5 \times 10^{13}$ G	1414.45	2827.94	5665.37	11395
$B = 10^{14}$ G	2141.17	4275.51	8543.9	17099.7
$B = 5 \times 10^{14}$ G	5619.96	11214.2	22378.9	44666.1

As L increases, dT/dr near the surface increases. The value of dT/dr near the surface also increases with the increase in B whereas $r-T$ relation is almost linear, as for the non-magnetised case (or for $B \leqslant 10^9$ G).

Table 4: Interface radius (in R) for different luminosities and magnetic fields

L	$10^{-5}\,L_\odot$	$10^{-4}\,L_\odot$	$10^{-3}\,L_\odot$	$10^{-2}\,L_\odot$
$B=0$	0.9978	0.9958	0.9918	0.9844
$B=10^{10}$ G	0.9979	0.9959	0.9920	0.9846
$B=10^{11}$ G	0.9982	0.9963	0.9926	0.9855
$B=10^{12}$ G	0.9991	0.9978	0.9949	0.9888
$B=5\times10^{12}$ G	0.99975	0.999256	0.99788	0.994272
$B=10^{13}$ G	0.99987	0.9996	0.9988	0.9965
$B=5\times10^{13}$ G	0.999972	0.999914	0.999732	0.999166
$B=10^{14}$ G	0.999986	0.999958	0.999866	0.999576
$B=5\times10^{14}$ G	0.999998	0.999992	0.999972	0.999914

3.2 Varying magnetic field

It is generally believed that the magnetic field strength at the surface of a white dwarf is several orders of magnitude smaller than the central field strength. Therefore, in this section we consider a more realistic density dependent magnetic field profile such that the magnetic field strength decays from the core of the white dwarf to its surface. We choose L such that $10^{-5}L_\odot \leqslant L \leqslant 10^{-2}L_\odot$ and vary the magnitudes of B_s and B_0, keeping η and γ constant, to investigate how T_*, r_* and temperature profile change.

The calculations done in this section are very similar to those of §3.1 except that $\frac{d}{dT}\left(\frac{B^2}{8\pi}\right) \neq 0$ in Eqn. (23). As earlier, we substitute P in terms of ρ in Eqn. (23) using the ideal gas equation of state to obtain

$$\frac{d}{dT}\left(\frac{\rho k_B T}{\mu m_\mu}+\frac{B^2}{8\pi}\right)=\frac{4ac}{3}\frac{4\pi GM}{\kappa_0 L}\frac{T^{6.5}}{\left(\rho+\frac{B^2}{8\pi c^2}\right)}. \tag{29}$$

Putting in the values of the constants and substituting $Z=0.1$ and $X=0$, we obtain

$$5.938\times10^7\rho+5.938\times10^7 T\frac{d\rho}{dT}+0.0796B\frac{dB}{d\rho}\frac{d\rho}{dT}=\frac{1.168}{L}\frac{T^{6.5}}{\left(\rho+\frac{B^2}{2.261\times10^{22}}\right)}. \tag{30}$$

Eqns. (27) and (30) are simultaneously solved by specifying boundary conditions at the surface as before: $\rho(T_s)=10^{-10}\,\mathrm{g\,cm^{-3}}$ and $r(T_s)=R=5000$ km, where $T_s=5000$ K. The values of T_*, ρ_* and r_* are obtained from the $\rho-T$ and $r-T$ profiles in the same way as in the case of constant field, as shown in Figs. 9, 10, 11 and 12. Tables 5, 6 and 7 show T_*, ρ_* and r_* respectively, for various values of $B\equiv(B_s,B_0)$ and L.

Table 5: Interface temperature (in K) for different luminosities and magnetic fields

L	$10^{-5}\,L_\odot$	$10^{-4}\,L_\odot$	$10^{-3}\,L_\odot$	$10^{-2}\,L_\odot$
$B=(0,0)$	2.332×10^6	4.50238×10^6	8.69273×10^6	1.6783×10^7
$B=(10^9\text{ G},10^{14}\text{ G})$	2.44368×10^6	4.61565×10^6	8.81325×10^6	1.69275×10^7
$B=(10^9\text{ G},5\times10^{14}\text{ G})$	2.81701×10^6	5.1498×10^6	9.65885×10^6	1.84453×10^7
$B=(10^{10}\text{ G},10^{13}\text{ G})$	2.43875×10^6	4.60434×10^6	8.78775×10^6	1.68706×10^7
$B=(10^{10}\text{ G},10^{14}\text{ G})$	2.98466×10^6	5.25529×10^6	9.50633×10^6	1.76262×10^7
$B=(10^{10}\text{ G},5\times10^{14}\text{ G})$	3.93081×10^6	6.6721×10^6	1.15646×10^7	2.06066×10^7
$B=(10^{11}\text{ G},10^{13}\text{ G})$	2.98321×10^6	5.24806×10^6	9.48594×10^6	1.75755×10^7
$B=(10^{11}\text{ G},10^{14}\text{ G})$	4.4574×10^6	7.43835×10^6	1.25587×10^7	2.15789×10^7
$B=(10^{11}\text{ G},5\times10^{14}\text{ G})$	6.21249×10^6	1.02625×10^7	1.70449×10^7	2.85704×10^7
$B=(10^{12}\text{ G},10^{14}\text{ G})$	7.3182×10^6	1.19236×10^7	1.95736×10^7	3.23512×10^7
$B=(10^{12}\text{ G},5\times10^{14}\text{ G})$	1.02447×10^7	1.6724×10^7	2.74177×10^7	4.51058×10^7
$B=(10^{13}\text{ G},5\times10^{14}\text{ G})$	2.10308×10^7	3.18665×10^7	4.91886×10^7	7.74337×10^7

From Table 5, we see that T_* increases with increasing B_s, B_0 and L. For a given (B_s,B_0), T_* increases as L increases.

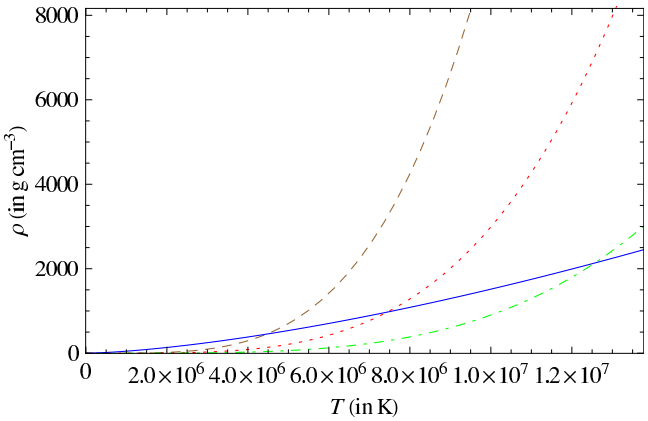

Figure 9. Variation of density with temperature for $B = (B_s, B_0) = (10^{11}\,\mathrm{G}, 10^{14}\,\mathrm{G})$ and different luminosities: $10^{-5}\,L_\odot$ (dashed line), $10^{-4}\,L_\odot$ (dotted line) and $10^{-3}\,L_\odot$ (dot-dashed line). ρ_* and T_* are obtained from the intersection of the $\rho - T$ profiles with Eqn. (4) (solid line).

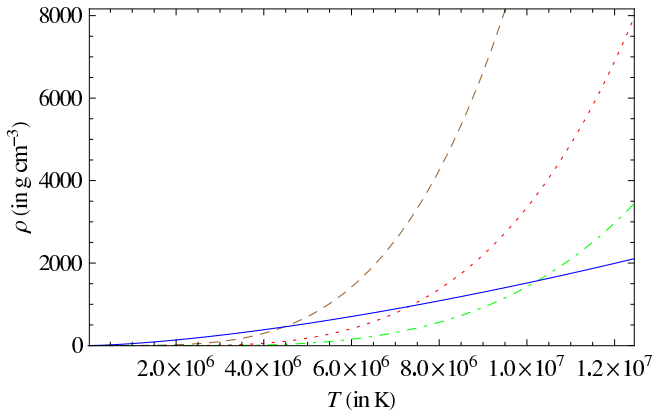

Figure 10. Variation of density with temperature for $L = 10^{-5}\,L_\odot$ and different magnetic fields: $(10^{11}\,\mathrm{G}, 10^{14}\,\mathrm{G})$ (dashed line), $(10^{12}\,\mathrm{G}, 10^{14}\,\mathrm{G})$ (dotted line) and $(10^{12}\,\mathrm{G}, 5\times10^{14}\,\mathrm{G})$ (dot-dashed line). ρ_* and T_* are obtained from the intersection of the $\rho - T$ profiles with Eqn. (4) (solid line).

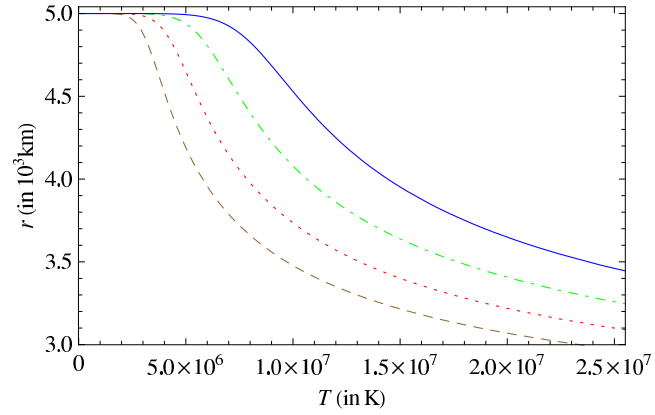

Figure 11. Variation of radius with temperature for $B = (10^{12}\,\mathrm{G}, 10^{14}\,\mathrm{G})$ and different luminosities: $10^{-5}\,L_\odot$ (dashed line), $10^{-4}\,L_\odot$ (dotted line), $10^{-3}\,L_\odot$ (dot-dashed line) and $10^{-2}\,L_\odot$ (solid line).

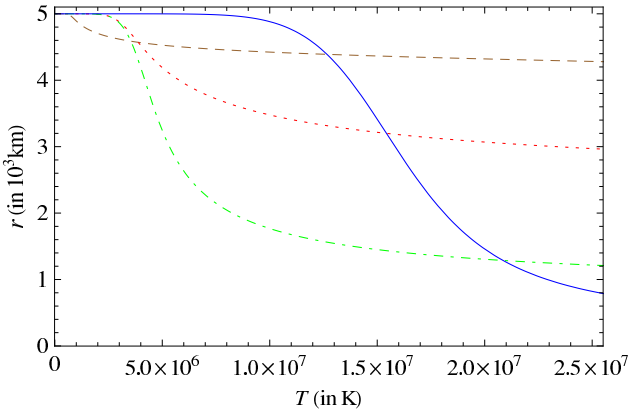

Figure 12. Variation of radius with temperature for $L = 10^{-5}\,L_\odot$ and different magnetic fields: $(10^{11}\,\mathrm{G}, 10^{14}\,\mathrm{G})$ (dashed line), $(10^{12}\,\mathrm{G}, 10^{14}\,\mathrm{G})$ (dotted line), $(10^{12}\,\mathrm{G}, 5\times10^{14}\,\mathrm{G})$ (dot-dashed line) and $(10^{13}\,\mathrm{G}, 5\times10^{14}\,\mathrm{G})$ (solid line).

However, the percentage change in T_* with the change in L decreases as B_s and B_0 increase. In other words, the increase of T_* due to the increase of L is somewhat saturated with the increase in $B = (B_s, B_0)$. Also, for a given B_s and B_0, r_* decreases with L. Therefore, the interface moves inwards with an increase in L for a given (B_s, B_0).

Table 6: Interface density (in $\mathrm{g\,cm^{-3}}$) for different luminosities and magnetic fields

L	$10^{-5}\,L_\odot$	$10^{-4}\,L_\odot$	$10^{-3}\,L_\odot$	$10^{-2}\,L_\odot$
$B = (0, 0)$	170.722	457.995	1228.66	3296.13
$B = (10^9\,\mathrm{G}, 10^{14}\,\mathrm{G})$	183.132	475.387	1254.3	3338.76
$B = (10^9\,\mathrm{G}, 5\times10^{14}\,\mathrm{G})$	226.663	560.252	1439.08	3797.74
$B = (10^{10}\,\mathrm{G}, 10^{13}\,\mathrm{G})$	182.578	473.641	1248.86	3321.95
$B = (10^{10}\,\mathrm{G}, 10^{14}\,\mathrm{G})$	247.196	577.555	1405.13	3547.6
$B = (10^{10}\,\mathrm{G}, 5\times10^{14}\,\mathrm{G})$	373.612	826.213	1885.37	4484.42
$B = (10^{11}\,\mathrm{G}, 10^{13}\,\mathrm{G})$	247.015	576.363	1400.61	3532.32
$B = (10^{11}\,\mathrm{G}, 10^{14}\,\mathrm{G})$	451.149	972.552	2133.61	4805.54
$B = (10^{11}\,\mathrm{G}, 5\times10^{14}\,\mathrm{G})$	742.329	1576.09	3373.56	7321.02
$B = (10^{12}\,\mathrm{G}, 10^{14}\,\mathrm{G})$	949.083	1973.82	4151.48	8821.32
$B = (10^{12}\,\mathrm{G}, 5\times10^{14}\,\mathrm{G})$	1571.98	3278.76	6882.48	14522.7
$B = (10^{13}\,\mathrm{G}, 5\times10^{14}\,\mathrm{G})$	4623.6	8623.83	16538.4	32665.8

$B = (10^{12}\ \mathrm{G}, 10^{14}\ \mathrm{G})$	0.7492	0.7158	0.6851	0.6560
$B = (10^{12}\ \mathrm{G}, 5 \times 10^{14}\ \mathrm{G})$	0.3485	0.3165	0.2907	0.2694
$B = (10^{13}\ \mathrm{G}, 5 \times 10^{14}\ \mathrm{G})$	0.2512	0.1892	0.1454	0.1152

As shown in Figs. 11 and 12, unlike the constant magnetic field case the $r - T$ profile is no longer linear for any L. Also, as L increases, dT/dr near the surface increases. The value of dT/dr also increases more with the increase in B_s as compared to increase in B_0. dT/dr near the surface is very high for $B_s \geqslant 10^{13}$ G and $B_0 \geqslant 10^{15}$ G. Therefore, the temperature fall near the surface increases for increasing strength of the magnetic field and luminosity, as for the previous cases. The values of ρ_* and r_* also increase and decrease respectively with the increase of L and/or B.

4 VARIATION OF LUMINOSITY WITH MAGNETIC FIELD

In this section, we determine how the luminosity of a white dwarf changes as the magnetic field strength increases such that,

1. the interface radius for a magnetised white dwarf is the same as that for a non-magnetised white dwarf i.e., $r_{*,B\neq0} = r_{*,B=0}$,
2. the interface temperature for a magnetised white dwarf is the same as that for a non-magnetised white dwarf i.e., $T_{*,B\neq0} = T_{*,B=0}$.

We also check if the conditions above can be satisfied simultaneously by changing the value of T_s accordingly. We calculate L for various magnetic field profiles, such that either r_* or T_* has the same value as that for the non-magnetised white dwarf with a luminosity $L = 10^{-5} L_\odot$.

4.1 Fixed interface radius

4.1.1 Constant magnetic field

Note that for $B = 0$ and $L = 10^{-5}\ L_\odot$, we have found $r_* = 0.9978\ R$, $\rho_* = 170.722\ \mathrm{g\,cm^{-3}}$ and $T_* = 2.332 \times 10^6$ K (from Table 1). We solve Eqns. (26) and (27) as done in §3.1, but this time we vary L in order to fix $r_* = 0.9978\ R$. We use the same boundary conditions as in Eqn. (28).

Table 8: Variation of luminosity with magnetic field for a fixed r_*

B (in G)	L (in $L_\odot$)	T_* (in K)	ρ_* (in g cm^{-3})
$B = 0$	10^{-5}	2.332×10^6	170.722
$B = 10^9$	1.045×10^{-5}	2.36151×10^6	174.401
$B = 10^{10}$	1.173×10^{-5}	2.4408×10^6	182.808
$B = 10^{11}$	1.882×10^{-5}	2.79632×10^6	224.17
$B = 10^{12}$	1.05×10^{-4}	4.74811×10^6	495.998
$B = 5 \times 10^{12}$	1.092×10^{-3}	1.09932×10^7	1747.37
$B = 10^{13}$	3.616×10^{-3}	1.74767×10^7	3502.58
$B = 5 \times 10^{13}$	7.305×10^{-2}	5.76089×10^7	17473.7

Table 8 shows that the luminosity has to increase with an increase in magnetic field strength if the interface is at the same radius. However, the increase in L is appreciable only for $B > 10^{11}$ G. The value of T_* also increases with an increase in B, which is expected as T_* is proportional to L.

4.1.2 Varying magnetic field

Here, we assume a magnetic field profile as given by Eqn. (24) and find the variation of luminosity with a change in B_s and B_0 so that the interface radius is same as for the non-magnetic case.

We solve Eqns. (27) and (30) as done in §3.2, but this time vary L in order to fix $r_* = 0.9978\ R$.

Table 9: Variation of luminosity with magnetic field for a fixed r_*

B (in G)	L (in $L_\odot$)	T_* (in K)	ρ_* (in g cm^{-3})

$B = (0, 0)$	10^{-5}	2.332×10^6	170.722
$B = (10^9, 10^{12})$	9.78×10^{-6}	2.3184×10^6	170.722
$B = (10^9, 10^{13})$	5.17×10^{-6}	1.94342×10^6	129.882
$B = (10^9, 5 \times 10^{13})$	2.87×10^{-8}	494967	16.6941
$B = (10^{10}, 10^{12})$	8.15×10^{-6}	2.21142×10^6	157.654
$B = (10^{10}, 5 \times 10^{12})$	1.35×10^{-6}	1.37434×10^6	77.2393
$B = (10^{10}, 10^{13})$	3.08×10^{-8}	542023	19.1304
$B = (10^{11}, 10^{13})$	2.33×10^{-13}	70709.3	0.901391

Interestingly, Table 9 shows that L and T_* both decrease as the magnetic field strength increases. However, the change is appreciable only for $B_s \geqslant 10^{10}$ G and $B_0 \geqslant 10^{12}$ G. The value of L becomes quite low $\sim 10^{-6}\, L_\odot$ and lower, for white dwarfs with (B_s, B_0) = (10^{10} G, 5×10^{12} G) and higher, which might make it difficult to detect such highly magnetised white dwarfs.

4.2 Fixed interface temperature

4.2.1 Constant magnetic field

First we look at white dwarfs with constant a magnetic field strength throughout. We solve Eqns. (26) and (27) as done in §3.1, but this time we vary L in order to fix $T_* = 2.332 \times 10^6$ K. We use the same boundary conditions as in Eqn. (28).

Table 10: Variation of luminosity with magnetic field for fixed T_*

B (in G)	L (in $L_\odot$)	ρ_* (in g cm^{-3})	r_*
$B = 0$	10^{-5}	170.722	0.9978 R
$B = 10^9$	10^{-5}	170.722	0.9978 R
$B = 10^{11}$	9.9583×10^{-6}	170.723	0.9982 R
$B = 10^{12}$	6.9672×10^{-6}	170.723	0.9992 R
$B = 5 \times 10^{12}$	8.079×10^{-7}	170.722	0.999926 R
$B = 10^{13}$	2.143×10^{-7}	170.722	0.99998 R
$B = 5 \times 10^{13}$	8.7423×10^{-9}	170.723	R
$B = 10^{14}$	2.1869×10^{-9}	170.723	R

Table 10 shows that unlike the case with fixed r_* and constant magnetic field, L here has to decrease with the increase in B. However, the decrease in L is significant only when $B \geqslant 5 \times 10^{12}$ G. For higher magnetic field strengths, the luminosity becomes very small and goes beyond the detection limit. Also, r_* gradually increases as B increases. This is because the rate of temperature fall with radius across the envelope is higher for higher fields (from Eqn. 27). Therefore, r_* has to increase for T_* to be constant.

4.2.2 Varying magnetic field

Here, we solve Eqns. (27) and (30) as done in §3.2, but this time we vary L to get $T_* = 2.332 \times 10^6$ K, using the same boundary conditions as in Eqn. (28).

Table 11: Variation of luminosity with magnetic field for a fixed T_*

B (in G)	L (in $L_\odot$)	ρ_* (in g cm^{-3})	r_*
$B = (0, 0)$	10^{-5}	170.722	0.9978 R
$B = (10^9, 10^{12})$	9.9823×10^{-6}	170.722	0.9978 R
$B = (10^9, 10^{14})$	8.4274×10^{-6}	170.722	0.9940 R
$B = (10^9, 5 \times 10^{14})$	4.7561×10^{-6}	170.722	0.97935 R
$B = (10^{10}, 10^{12})$	9.8251×10^{-6}	170.723	0.9977 R
$B = (10^{10}, 10^{13})$	8.4848×10^{-6}	170.723	0.9959 R
$B = (10^{10}, 10^{14})$	3.5514×10^{-6}	170.722	0.97857 R
$B = (10^{10}, 5 \times 10^{14})$	9.721×10^{-7}	170.722	0.90875 R

$B = (10^{11}, 10^{13})$	3.5439×10^{-6}	170.722	0.9896 R
$B = (10^{11}, 10^{14})$	5.1813×10^{-7}	170.723	0.9192 R
$B = (10^{11}, 5 \times 10^{14})$	1.07855×10^{-7}	170.723	0.69839 R
$B = (10^{12}, 10^{14})$	3.5327×10^{-8}	170.723	0.8414 R
$B = (10^{12}, 5 \times 10^{14})$	7.0921×10^{-9}	170.723	0.51559 R

Like the constant field case, we find that even for varying magnetic field strength, L has to decrease as B increases for T_* to be unchanged. From Table 11, we see that L becomes very small when $B_s > 10^{10}$ G and $B_0 \geqslant 10^{14}$ G. We also see that r_* decreases with increase in magnetic field strength.

4.3 Fixed interface radius, fixed interface temperature and varying surface temperature

We find that the $\rho - T$ and $r - T$ profiles are sensitive to T_s only for relatively low values of the magnetic field:

1. $B \leqslant 10^{10}$ G for constant magnetic field.
2. $B_s \leqslant 10^{10}$ G and $B_0 \leqslant 10^{12}$ G for a varying magnetic field.

Hence, for the larger values of B that we are considering, we do not have any considerable change in the values of T_* and r_* (as obtained for $T_s = 5000$ K), by changing T_s.

5 COOLING IN THE PRESENCE OF A MAGNETIC FIELD AND POST COOLING TEMPERATURE PROFILE

We know how to find the cooling timescale of a white dwarf if we know the $L - T$ relation, which was done in §2.2. In this section, we find the $L - T$ relations for the cases mentioned in §4 and using those relations, implement cooling with time to find the present interface temperature, $T_{*,pr}$ from the initial interface temperature, $T_{*,in}$, for $\tau = 10$ billion years. Once we know $T_{*,pr}$, we can easily calculate the present surface temperature, $T_{s,pr}$, using the equation for dT/dr relation and the present value of the luminosity $L_{*,pr}$.

5.1 Specific heat in the presence of magnetic field

A magnetic field can, in principle, affect the state of the ionic core and thus its thermodynamic properties, such as the specific heat. The relevant parameter to quantify this effect is

$$b = \frac{\omega_B}{\omega_p}, \tag{31}$$

where

$$\omega_B = \frac{ZeB}{Mc}, \quad \text{and} \quad \omega_p = \sqrt{\frac{4\pi Z^2 e^2 n}{M}}, \tag{32}$$

are the ion cyclotron and ion plasma frequencies, respectively. Here, n is the number density of the ions. As discussed in §2.2, ω_p is effectively the Debye frequency of the ionic lattice. We would expect the effect of the magnetic field on the ionic core to be strong when $b \geqslant 1$, i.e. when the cyclotron frequency is comparable to or larger than the Debye frequency of the lattice.

The effect of a magnetic field on a BCC Coulomb lattice has been studied by Baiko (2009), who concluded that there is an appreciable change of the specific heat only for $b \gg 1$ except when $T \ll \theta_D$. For the white dwarfs we consider, $B < 10^{12}$ G at the interface, which corresponds to $b \leqslant 1$. Further, the interface temperature is not significantly smaller than θ_D. Thus, we are justified in working with a value of the specific heat appropriate for a non-magnetised system despite the presence of a magnetic field.

It will be of interest to study the effect of much stronger magnetic fields on the ionic core and its specific heat. In particular, if the magnetic field is strong enough to cause Landau quantization of the electron gas in the core, it could result in a change in the effective ion-ion interaction as mediated by the electrons. This would be in addition to the direct effect of the field on the ionic core as described above. The effect of a magnetic field on the phonon spectrum of ions in conventional solid state systems has been investigated and found to be weak for practical values of the field appropriate to these systems (Holz 1972). However, in an astrophysical context, the effect might be appreciable if fields of the order of 10^{15} G arise and could result in very interesting physics. We defer an investigation of this to a future work.

Using the values of T_* for different L as obtained in §3, we can approximate L as a function of T_*. Once we know how

L varies with T_*, we can repeat the cooling calculations as done in §2.2 to first find $T_{*,pr}$ (after cooling) and then find $T_{s,pr}$, using the value of $L_{*,pr}$ in the dT/dr relation.

5.2 Fixed interface radius

5.2.1 Constant magnetic field

From Table 8, we know the values of $L_{*,in}$ and the $L-T$ relation can be found using Table 2. The calculated values of $T_{*,pr}$ and $T_{s,pr}$ for $r_* = 0.9978\ R$ are given in Table 12.

From Table 12, we see that as B increases, the coefficient in the $L-T$ relation decreases whereas the exponent of T increases. Also the cooling is enhanced for higher Bs. We see an appreciable reduction in T_* for $B > 10^{12}$ G. Hence, the change in B affects T_* considerably.

Table 12: Change in T_* with time due to the presence of a magnetic field for fixed r_* and $T_s = 5000$ K

B (in G)	$T_{*,in}$ (in K)	$L_{*,in}$ (in $L_\odot$)	L (in terms of T)	$T_{*,pr}$ (in K)
0	2.332×10^6	10^{-5}	$2.013 \times 10^6 T^{3.500}$	2.2232×10^6
10^9	2.36151×10^6	1.045×10^{-5}	$2.013 \times 10^6 T^{3.500}$	2.24814×10^6
10^{10}	2.4408×10^6	1.173×10^{-5}	$2.013 \times 10^6 T^{3.500}$	2.31443×10^6
10^{11}	2.79632×10^6	1.882×10^{-5}	$1.994 \times 10^6 T^{3.501}$	2.59905×10^6
10^{12}	4.74811×10^6	1.05×10^{-4}	$7.911 \times 10^5 T^{3.555}$	3.86949×10^6
5×10^{12}	1.09932×10^7	1.092×10^{-3}	$1.467 \times 10\, T^{4.183}$	7.18397×10^6
10^{13}	1.74767×10^7	3.616×10^{-3}	$1.355 \times 10^{-2} T^{4.558}$	1.01002×10^7
5×10^{13}	5.76089×10^7	7.305×10^{-2}	$1.265 \times 10^{-6} T^{4.943}$	2.27239×10^7

5.2.2 Varying magnetic field

We find the $L-T$ relations for different values of B using Table 5. We also know the values of $L_{*,in}$ for different field strengths from Table 9. Using these, we calculate $T_{*,pr}$ and then $T_{s,pr}$ for different values of B, as given in Table 13.

Table 13: The change in T_* with time due to the presence of a magnetic field for a fixed r_* and $T_s = 5000$ K

B (in G)	$T_{*,in}$ (in K)	$L_{*,in}$ (in $L_\odot$)	L (in terms of T)	$T_{*,pr}$(in K)
$(0, 0)$	2.332×10^6	10^{-5}	$2.013 \times 10^6 T^{3.500}$	2.2232×10^6
$(10^9, 10^{12})$	2.3184×10^6	9.78×10^{-6}	$2.002 \times 10^6 T^{3.500}$	2.21225×10^6
$(10^9, 10^{13})$	1.94342×10^6	5.17×10^{-6}	$1.905 \times 10^6 T^{3.503}$	1.88494×10^6
$(10^9, 5 \times 10^{13})$	4.94967×10^5	2.87×10^{-8}	$2.622 \times 10^5 T^{3.633}$	4.94599×10^5
$(10^{10}, 10^{12})$	2.21142×10^6	8.15×10^{-6}	$1.905 \times 10^6 T^{3.503}$	2.12125×10^6
$(10^{10}, 5 \times 10^{12})$	1.37434×10^6	1.35×10^{-6}	$1.533 \times 10^6 T^{3.516}$	1.35709×10^6
$(10^{10}, 10^{13})$	5.42023×10^5	3.08×10^{-8}	$5.588 \times 10^4 T^{3.733}$	541630
$(10^{11}, 10^{13})$	7.07093×10^4	2.33×10^{-13}	$3.411 \times 10^1 T^{4.179}$	70709.3

Unlike the constant field case, here L decreases with increasing B. With the increase of field strength, the coefficient in the $L-T$ relation decreases whereas the exponent increases. Unlike the constant field case, increasing B results in slower cooling. However, as before, T_s is not affected much by the increase of field strength.

5.3 Fixed interface temperature

5.3.1 Constant magnetic field

We find the $L-T$ relations for different values of B using Table 2 and then use Table 10 to obtain the values of $L_{*,in}$ for different fields. The values of $T_{*,pr}$ and $T_{s,pr}$ calculated for different fields are given in Table 14.

Table 14: The change in T_* with time due to the presence of a magnetic field for a fixed T_* and $T_s = 5000$ K

B (in G)	$T_{*,in}$ (in K)	$L_{*,in}$ (in $L_\odot$)	L (in terms of T)	$T_{*,pr}$ (in K)
0	2.332×10^6	10^{-5}	$2.013 \times 10^6 T^{3.500}$	2.223×10^6
10^9	2.332×10^6	10^{-5}	$2.013 \times 10^6 T^{3.500}$	2.223×10^6
10^{11}	2.332×10^6	9.9583×10^{-6}	$1.890 \times 10^6 T^{3.504}$	2.224×10^6
10^{12}	2.332×10^6	6.9672×10^{-6}	$1.502 \times 10^4 T^{3.810}$	2.262×10^6
5×10^{12}	2.332×10^6	8.079×10^{-7}	$4.875 \times 10^{-3}\ T^{4.686}$	2.325×10^6
10^{13}	2.332×10^6	2.143×10^{-7}	$1.066 \times 10^{-4} T^{4.857}$	2.330×10^6
5×10^{13}	2.332×10^6	8.7423×10^{-9}	$6.210 \times 10^{-7} T^{4.985}$	2.332×10^6
10^{14}	2.332×10^6	2.1869×10^{-9}	$1.350 \times 10^{-7} T^{4.994}$	2.332×10^6

From Table 14, we find that the coefficient in the $L - T$ relation decreases and the exponent of T increases with the increase of B. Also the cooling rate decreases with the increase of field strength and T_* is almost unchanged even after $\tau = 10$ billion years for $B \geqslant 10^{13}$ G.

5.3.2 Varying magnetic field

The $L - T$ relations for different values of B are obtained using Table 5 and the values of $L_{*,in}$ for different fields are obtained from Table 11. We then calculate $T_{*,pr}$ and $T_{s,pr}$ for the different values of B given in Table 15.

As for constant field, an increase of the magnetic field strength results in a decrease in the coefficient and increase in the exponent of T in the $L - T$ relation, as shown in Table 15. In this case as well, the cooling rate decreases appreciably with an increase in magnetic field strength for $B_s \geqslant 10^{11}$ G and $B_0 \geqslant 10^{14}$ G.

Table 15: The change in T_* with time due to the presence of magnetic field for a fixed T_* and $T_s = 5000$ K

B (in G)	$T_{*,in}$ (in K)	$L_{*,in}$ (in $L_\odot$)	L (in terms of T)	$T_{*,pr}$ (in K)
$(0, 0)$	2.332×10^6	10^{-5}	$2.013 \times 10^6 T^{3.500}$	2.223×10^6
$(10^9, 10^{12})$	2.332×10^6	9.9823×10^{-6}	$2.002 \times 10^6 T^{3.500}$	2.224×10^6
$(10^9, 10^{14})$	2.332×10^6	8.4274×10^{-6}	$7.102 \times 10^5 T^{3.562}$	2.238×10^6
$(10^9, 5 \times 10^{14})$	2.332×10^6	4.7561×10^{-6}	$9.652 \times 10^4 T^{3.666}$	2.274×10^6
$(10^{10}, 10^{12})$	2.332×10^6	9.8251×10^{-6}	$1.794 \times 10^6 T^{3.507}$	2.225×10^6
$(10^{10}, 10^{13})$	2.332×10^6	8.4848×10^{-6}	$6.877 \times 10^5 T^{3.565}$	2.237×10^6
$(10^{10}, 10^{14})$	2.332×10^6	3.5514×10^{-6}	$2.040 \times 10^3 T^{3.910}$	2.291×10^6
$(10^{10}, 5 \times 10^{14})$	2.332×10^6	9.721×10^{-7}	$7.268 \times 10^{-1} T^{4.356}$	2.323×10^6
$(10^{11}, 10^{13})$	2.332×10^6	3.5439×10^{-6}	$1.309 \times 10^2 T^{4.088}$	2.298×10^6
$(10^{11}, 10^{14})$	2.332×10^6	5.1813×10^{-7}	$1.753 \times 10^{-2} T^{4.564}$	2.328×10^6
$(10^{11}, 5 \times 10^{14})$	2.332×10^6	1.07855×10^{-7}	$1.675 \times 10^{-3} T^{4.617}$	2.331×10^6
$(10^{12}, 10^{14})$	2.332×10^6	3.5327×10^{-8}	$1.588 \times 10^{-5} T^{4.864}$	2.332×10^6
$(10^{12}, 5 \times 10^{14})$	2.332×10^6	7.0921×10^{-9}	$1.534 \times 10^{-6} T^{4.912}$	2.332×10^6

5.4 Fixed interface radius, fixed interface temperature and varying surface temperature

As discussed in §4.3, the $\rho - T$ and $r - T$ profiles are sensitive to T_s only at relatively low values of B. Hence, for larger values of B, we do not have any considerable change in the values of T_* and r_* (as obtained for $T_s = 5000$ K), by changing T_s. Therefore, we do not calculate the cooling rates for this case as the change in T_* is observable only for smaller values of B, which is the same as the non-magnetic result.

6 DISCUSSION

In this section, we discuss our results described in the previous sections and their physical significance.

6.1 Non-magnetised white dwarfs

From Table 1, we see that as L increases in the envelope, T_* and ρ_* both increase whereas r_* decreases. Using Eqns. (4), (5) and (6), we obtain

$$L \propto T_*^{3.5},\ \rho_* \propto T_*^{3/2},\ \text{and}\ (T_* - T_s) \propto \left(\frac{R}{r_*} - 1\right). \tag{33}$$

Hence, a white dwarf having a larger T_* has more stored thermal energy, which it can radiate thus giving rise to a larger L. Also, a larger T_* corresponds to a larger ρ_*. For a fixed T_s and R, r_* should decrease as T_* increases. This is because the outer regions of the white dwarf are cooler as compared to the inner ones.

We also find that $|\Delta T/\Delta r|$, i.e., $|(T_s - T_*)/(R - r_*)|$ and the cooling rate $\Delta T/\Delta t$ increase with the increase in luminosity of the white dwarf. From Eqns. (6) and (15),

$$\frac{\Delta T}{\Delta r} = \left(\frac{T_* - T_s}{R - r_*}\right),\ \text{and}\ (\mathrm{T}^{-5/2} - \mathrm{T}_0^{-5/2}) \propto \tau. \tag{34}$$

Note that L corresponds to the energy flux which is transported across a spherical surface and hence a larger luminosity means a larger flux (for a given radius) i.e. a larger $\Delta T/\Delta r$. From Eqn. (34) it is clear that hotter or more luminous white dwarfs cool faster as T_0 is larger. Therefore, the cooling rate should be more for a white dwarf having larger luminosity.

6.2 Magnetised white dwarfs having fixed interface radius

In §4.1, we have found out how much the luminosity has to increase or decrease for a magnetised white dwarf for it to have the same interface radius as a non-magnetised white dwarf. Then in §5.1, we have also computed the cooling rates for the corresponding cases and used the values of L as obtained in §4.1 to obtain the surface temperatures. Here we discuss our results.

6.2.1 Constant magnetic field

For a fixed r_* and constant B, we have computed $T_{*,in}$, ρ_*, $T_{*,pr}$ and $T_{s,pr}$. We have fixed $r_* = 0.9978\ R$, corresponding to $L = 10^{-5}\ L_\odot$ for the non-magnetic case. We have found that as B increases, L, T_* and ρ_* all have to increase for r_* to be fixed, which can be seen from Table 8. From Eqn. (26), we have

$$\frac{d\rho}{dT} \propto \frac{1}{T}\left(\frac{1.168}{L}\frac{T^{6.5}}{\left(\rho + \frac{B^2}{8\pi c^2}\right)} - 5.938 \times 10^7 \rho\right). \tag{35}$$

From Eqn. (35), we see that if B increases, then $d\rho/dT$ decreases for a given T and L. As the initial conditions are the same, we obtain a smaller value of ρ for a given T, if B is larger. Hence, the presence of magnetic field suppresses the matter density at a given temperature. As a result, T_*, which is obtained by the intersection of the $\rho - T$ curve with Eqn. (4), increases. This is because the density of matter at which it becomes degenerate is reached only at a higher temperature. Similarly, an increase of L also leads to the increase of T_*. Therefore, the increase of B leads to the increase of T_* and L. Also, ρ_* increases as $\rho_* \propto T_*^{3/2}$ by Eqn. (4).

We find that the temperature falls with radial distance from the centre of the white dwarf. $|\Delta T/\Delta r|$, and the rate of cooling of the white dwarf, i.e., $\Delta T/\Delta t$, both increase with B. As T_* increases with increasing B and L and r_* remain fixed, an increase in $|\Delta T/\Delta r|$ is expected. We have L to be of the form αT^γ, where α and γ are constants which depend on the magnetic field strength, as given in Table 12. With the increase of B, α decreases and γ increases. Hence, we have

$$-\frac{d}{dt}\left(\frac{3k_B T}{A m_\mu}\right) = \alpha T^\gamma, \tag{36}$$

which gives

$$\tau = \frac{3k_B}{A m_\mu}\frac{(T^{1-\gamma} - T_0^{1-\gamma})}{\alpha(\gamma - 1)}. \tag{37}$$

When B increases, $\alpha(\gamma - 1)$ decreases but $(T^{1-\gamma} - T_0^{1-\gamma})$ decreases more such that their ratio decreases. This is because T_0 increases more in comparison to T with increasing B, as can be seen from Table 12. Therefore, the cooling rate increases with the increase of B.

6.2.2 Varying magnetic field

In §4.1.2 and §5.2.2, we have fixed r_* for a varying magnetic field and calculated $T_{*,in}$, $T_{*,pr}$, ρ_* and $T_{s,pr}$. We have used $r_* = 0.9978\ R$, i.e. the value of interface radius corresponding to $B = 0$ and $L = 10^{-5}\ L_\odot$. From Table 9, we have seen that

as B increases, L, T_* and ρ_* all decrease for r_* to be fixed. This is the opposite of what is observed for a constant magnetic field.

From Eqn. (30) we have,

$$\frac{d\rho}{dT} = \frac{\left(\frac{1.168}{L}\frac{T^{6.5}}{\left(\rho+\frac{B^2}{8\pi c^2}\right)} - 5.938\times10^7\rho\right)}{\left(5.938\times10^7 T + 0.0796B\frac{dB}{d\rho}\right)}. \tag{38}$$

It can be seen that Eqn. (38) is quite similar to Eqn. (35), with the denominator having an additional term in Eqn. (38). For the B configuration that we have considered, the strength of the field increases with density. Therefore, $BdB/d\rho$ is positive and we obtain a smaller value of $d\rho/dT$ for a given field strength for the varying magnetic field case as compared to the one with a constant magnetic field. Therefore, a varying magnetic field suppresses the matter density at a given temperature more than a constant field and we obtain a larger value of T_*, for a similar reason as the constant field case. However, it should be noted that r_* also decreases such that $\Delta T/\Delta r$ decreases. From Eqn. (27),

$$\frac{dT}{dr} \propto \frac{\left(\rho+\frac{B^2}{8\pi c^2}\right)^2}{T^{6.5}}\frac{L}{r^2}. \tag{39}$$

In this case, the decrease in ρ with the increase in B is large enough to counteract an increase in ρ_B and dT/dr decreases with the increase in B for sufficiently small L. This does not happen in the constant field case as the reduction of ρ is not large enough and dT/dr near the interface increases with increasing B. Therefore, in this case we have a smaller T_* and a smaller L for larger field strengths, for r_* to be constant. The value of ρ_* also decreases with field as $\rho_* \propto T_*^{3/2}$.

We find that $|\Delta T/\Delta r|$ and $\Delta T/\Delta t$ both decrease with B. As T_* decreases with the increase in B and r_* remains fixed, a decrease in $|\Delta T/\Delta r|$ is expected. As for the previous case, L is of the form αT^γ as given in Table 13. Hence, we have

$$\tau \propto \frac{(T^{1-\gamma} - T_0^{1-\gamma})}{\alpha(\gamma-1)}. \tag{40}$$

When B increases, $\alpha(\gamma-1)$ and $(T^{1-\gamma}-T_0^{1-\gamma})$ both decrease. However, the decrease in $\alpha(\gamma-1)$ is more such that τ increases. With increasing B, T_0 and γ do not change considerably whereas α decreases by orders of magnitude. Therefore, the cooling rate decreases with the increase in B.

6.3 Magnetised white dwarfs with fixed interface temperature

In §4.2, we have computed the change of L of a magnetised white dwarf for it to have the same T_* as a non-magnetised white dwarf. Then in §5.3, we have found the cooling rates for the corresponding cases and used the values of L as obtained in §4.2 to obtain T_s. Here we discuss our results.

6.3.1 Constant magnetic field

For a fixed T_* and constant magnetic field, we have computed $T_{*,in}$, r_*, ρ_* and $T_{*,pr}$. We have fixed $T_* = 2.332\times10^6\,K$, which is the interface temperature corresponding to $L = 10^{-5}\,L_\odot$ for the non-magnetic case. We have found that as B increases, L decreases and r_* increases whereas ρ_* is constant, as can be seen from Table 10. From Eqns. (26) and (27), we have

$$\frac{d\rho}{dT} \propto \frac{1}{T}\left(\frac{1.168}{L}\frac{T^{6.5}}{\left(\rho+\frac{B^2}{8\pi c^2}\right)} - 5.938\times10^7\rho\right), \tag{41}$$

and

$$\frac{dr}{dT} \propto \frac{T^{6.5}}{\left(\rho+\frac{B^2}{8\pi c^2}\right)^2}\frac{r^2}{L}. \tag{42}$$

As $\rho_* \propto T_*^{3/2}$ for a nondegenerate envelope, ρ_* has to be fixed because T_* is fixed. We know from §6.2 that the presence of a magnetic field suppresses the matter density for a given T. As the initial conditions for the $\rho - T$ profile are the same, $d\rho/dT$ has to be larger near the interface for the magnetic case, which is achieved by the reduction of L. Therefore, for T_* to be fixed with increasing field, L should decrease.

Again as the initial conditions for solving Eqn. (42) are the same as for the non-magnetic case, dr/dT should be higher near the interface for obtaining higher r_* for a given T_*. This is achieved as the decrease in L is sufficiently small in comparison to the increase in ρ_B such that dr/dT near the interface increases and we obtain a larger value for r_*. An increase in $|\Delta T/\Delta r|$ is expected as T_* is fixed whereas r_* increases.

We find that the cooling rate $\Delta T/\Delta t$ decreases with the increase of the magnetic field strength. As in §6.2, L can be

written as αT^{γ} as given in Table 14 and the expression for the cooling timescale is given by Eqn. (37). Unlike the fixed r_* and constant field case, here the decrease in $(T^{1-\gamma} - T_0^{1-\gamma})$ is not as much as that for $\alpha(\gamma-1)$ which makes τ larger for larger B. As mentioned earlier in §6.2, α changes by orders of magnitude whereas T_0 and γ do not change considerably.

6.3.2 Varying magnetic field

In §4.2.2 and §5.3.2, we have fixed T_* for a varying magnetic field and calculated $T_{*,in}$, r_*, ρ_* and $T_{*,pr}$. We have fixed $T_* = 2.332 \times 10^6$ K, which is the interface temperature corresponding to $L = 10^{-5}\ L_\odot$ for the non-magnetic case and found that as B increases, both L and r_* decrease, whereas ρ_* remains constant, as can be seen from Table 11. We recall Eqns. (38) and (39) which are applicable here as well.

As $\rho_* \propto T_*^{3/2}$ for a nondegenerate envelope, ρ_* has to be fixed as T_* is fixed. Also, we know from §6.2 that a magnetic field suppresses ρ for a given T. As the initial conditions for the $\rho - T$ profile are same, we should have larger $d\rho/dT$ near the interface for the magnetic case, which happens because of a reduction in L. Therefore, for T_* to be fixed with increasing field, L has to decrease.

Now, as the initial conditions for solving Eqn. (39) are the same as those for the non-magnetic case and dT/dr near the surface is larger for larger magnetic fields (from Fig. 12), dT/dr should be smaller near the interface for obtaining a smaller value of r_* for a given T_* in this case. We find that with increasing B, the luminosity for the varying field is sufficiently small in addition to ρ being small, which counteracts the increase in ρ_B thus making dT/dr near the interface smaller. Therefore, r_* decreases with increasing B for fixed T_*. $\Delta T/\Delta r$ decreases as T_* is fixed whereas r_* decreases.

We find that the cooling rate $\Delta T/\Delta t$ decreases as magnetic field strength increases. We have, $L = \alpha T^{\gamma}$ as given in Table 15 and the expression for the cooling timescale is given by Eqn. (37). As for the constant field and fixed T_* case, here the decrease in $\alpha(\gamma-1)$ is larger as compared to the decrease in $(T^{1-\gamma} - T_0^{1-\gamma})$, which makes τ larger for larger B.

6.4 Highly magnetised white dwarfs and their invisibility

For the solar neighbourhood of radius $R_0 \sim 8.0$ kpc and disk thickness $t \sim 0.5$ kpc, the expected number of visible white dwarfs with number density 1.5×10^{-2} pc^{-3} (Shapiro & Teukolsky 1983) is

$$N_{vis,wd} = \pi \times R_0^2 \times t \times 1.5 \times 10^{-2}\ \mathrm{pc}^{-3} \approx 1.5 \times 10^9. \tag{43}$$

As the average mass of observed white dwarfs is 0.6 $M_\odot$, the mass of these white dwarfs in the solar neighbourhood is

$$M_{vis,wd} = 0.6\ M_\odot \times 1.5 \times 10^9 = 9 \times 10^8\ M_\odot. \tag{44}$$

Now, 97% of the main sequence stars, with density in the solar neighbourhood $0.064\, M_\odot\ \mathrm{pc}^{-3}$, ultimately turn out to be white dwarfs. Hence the upper limit of total mass due to white dwarfs in the solar neighbourhood is given by

$$M_{total,wd} = \pi \times R_0^2 \times t \times 0.97 \times 0.064\ M_\odot\ \mathrm{pc}^{-3} \approx 6.24 \times 10^9\ \mathrm{M}_\odot. \tag{45}$$

From Eqns. (44) and (45), we have an approximate estimate of mass corresponding to non-visible white dwarfs

$$M_{non-vis,wd} = M_{total,wd} - M_{vis,wd} = 5.34 \times 10^9\ M_\odot. \tag{46}$$

Interestingly, this is the same order as the missing mass, of density $\sim 0.02\ M_\odot\ \mathrm{pc}^{-3}$, in the solar neighbourhood, which is $M_{missing} = \pi \times R_0^2 \times t \times 0.02\ M_\odot\ \mathrm{pc}^{-3} \approx 2 \times 10^9\ \mathrm{M}_\odot$.

Now, observed white dwarfs have luminosities in the range $\sim 10^{-5}\, L_\odot - 10^{-2}\, L_\odot$. In §4, we have shown that the luminosity of a magnetised white dwarf has to decrease for either r_* or T_* to be the same as a non-magnetised white dwarf, except for the case when there is a uniform magnetic field inside the white dwarf and r_* is fixed. In other words, for a magnetised white dwarf to have similar interface parameters as a non-magnetised one, its luminosity needs to be much smaller – the luminosity can be as small as $\sim 10^{-9}\ L_\odot$ for very high magnetic fields. Indeed the surface temperatures of white dwarfs with different B are found/observed neither to be coherently changing with B nor to be differing significantly for different B (e.g. Koester & Chanmugam 1990). Such low luminosity white dwarfs are naturally not visible. Above estimate argues that such highly magnetised white dwarfs may be a significant component of $M_{non-vis,wd}$. Like neutron stars, they are supposed to be in the very bottom left of the H-R diagram and hardly visible.

7 SUMMARY AND CONCLUSION

We have investigated the effects of magnetic field in the luminosity and cooling of white dwarfs. To the best of our knowledge, this is the first systematic attempt towards this mission. This is very useful to account for observability of recently proposed highly magnetised white dwarfs, in particular the ones having central field 5×10^{14} G. However, we have deferred our

investigation for white dwarfs with fields $\gtrsim 10^{15}$ G for a future work, which will affect the EoS significantly and, subsequently, might change the thermal conduction and, hence, observable properties more severely.

We have computed the variation of luminosity of highly magnetised white dwarfs with magnetic field strength (both radially constant and varying cases) and evaluated the corresponding cooling timescales for white dwarfs having fixed interface radius or temperature. Except for the fixed interface radius with constant magnetic field cases, we have seen that the luminosity is suppressed with the increase in field strength, in addition to a reduction of cooling rates (marginally). Therefore, white dwarfs with higher magnetic fields have lower luminosities and slower cooling, for the interface radius or temperature to be fixed.

For a similar gravitational energy (similar mass and radius), an increasing magnetic energy necessarily requires decreasing thermal energy for white dwarfs to be in equilibrium, which results in a decreasing luminosity. We have found that the luminosity could be as low as $\sim 10^{-8}\ L_\odot$ for a white dwarf with the central field $\sim 5 \times 10^{14}$ G and the surface field $\sim 10^{12}$ G, for a fixed interface temperature. As a result, such white dwarfs appear to be invisible with respect to current astronomical techniques. With decreasing the surface field, while the luminosity tends to be in the observable limit, it is still $\sim 10^{-6}\ L_\odot$ for the surface field $\sim 10^9$ G. For a fixed interface radius, however, luminosity could be much lower, $\sim 10^{-13}\ L_\odot$, for central and surface fields respectively $\sim 10^{13}$ G and $\sim 10^{11}$ G. By decreasing surface field to $\sim 10^9$ G, it is still $\sim 10^{-8}\ L_\odot$, well below the observational limit. Therefore, such white dwarfs, while expected to be present in the universe, are virtually invisible to us, perhaps lying in the lower left corner in the H-R diagram.

ACKNOWLEDGMENTS

We thank Chanda J. Jog of IISc for discussion and continuous encouragement.

REFERENCES

Adam D., 1986, A&A, 160, 95
Bahcall J. N., Soneira R. M., 1980, ApJS, 44, 73
Baiko D. A., 2009, Phys. Rev. E, 80, 046405
Bandyopadhyay D., Chakrabarty S., Pal S., 1997, Phys. Rev. Lett., 79, 2176
Chandrasekhar S., 1931, ApJ, 74, 81
Chandrasekhar S., 1931, MNRAS, 91, 456
Das U., Mukhopadhyay B., 2012, Phys. Rev. D, 86, 042001
Das U., Mukhopadhyay B., 2013, Phys. Rev. Lett., 110, 071102
Das U., Mukhopadhyay B., Rao A. R., 2013, ApJ, 767, L14
Das U., Mukhopadhyay B., 2014a, JCAP, 06, 050
Das U., Mukhopadhyay B., 2014b, MPLA, 29, 1450035
Das U., Mukhopadhyay B., 2015, JCAP, 05, 016
Fontaine G., Van Horn H. M., 1976, ApJS, 31, 467
Hachisu I., 1986, ApJS, 61, 479
Hansen B. M. S., 1999, ApJ, 520, 680
Holz A., 1972, ll Nuovo Cimento B, 9, 83
Howell D. A. et al., 2006, Nature, 443, 308
Koester, D., Chanmugam, G., 1990, Rep. Prog. Phys., 53, 837
Krisciunas K., 1977, AJ, 82, 195
Kundu A., Mukhopadhyay B., 2012, MPLA, 27, 1250084
Lamb D. Q., Van Horn H. M., 1975, ApJ, 200, 306
Lindemann F. A., 1910, Phys. Rev. Z, 11, 609
Mestel L., 1952, MNRAS, 112, 583
Mestel L., Ruderman M. A., 1967, MNRAS, 136, 27
Ostriker J. P., Hartwick F. D. A., 1968, ApJ, 153, 797
Subramanian S., Mukhopadhyay B., 2015, MNRAS *to appear* arXiv:1507.01606
Scalzo R. A. et al., 2010, ApJ, 713, 1073
Schmidt G. D. et al., 2003, ApJ, 595, 1101
Schwarzschild M., 1958, Structure and Evolution of the Stars, Princeton Univ. Press, Princeton, NJ
Shapiro S. L., Teukolsky S. A., 1983, Black Holes, White Dwarfs, and Neutron Stars: The Physics of Compact Objects, Wiley, New York

Sinha M., Mukhopadhyay B., Sedrakian A., 2013, Nucl. Phys. A, 898, 43
Spitzer L., 1978, Physical Processes in the Interstellar Medium, Wiley, New York
Tutukov A., Yungelson L., 1996, MNRAS, 280, 1035
Valyavin G. G., Shulyak D., Wade G. A. et al., 2014, Nature, 515, 88
Yoon S.-C., Langer N., 2004, A&A, 419, 623